Steroids 153 (2020) 108534

Contents lists available at ScienceDirect

Steroids

journal homepage: www.elsevier.com/locate/steroids

New steroidal oxazolines, benzoxazoles and benzimidazoles related to abiraterone and galeterone

Alexandra S. Latysheva[a], Vladimir A. Zolottsev[a], Alexander V. Veselovsky[a], Kirill A. Scherbakov[a], Galina E. Morozevich[a], Vadim S. Pokrovsky[a,b,c,*], Roman A. Novikov[d], Vladimir P. Timofeev[d], Yaroslav V. Tkachev[d], Alexander Y. Misharin[a]

[a] Orekhovich Institute of Biomedical Chemistry, Moscow, Russia
[b] N.N. Blokhin Cancer Research Center, Moscow, Russia
[c] RUDN University, Moscow, Russia
[d] Engelhardt Institute of Molecular Biology RAS, Moscow, Russia

ARTICLE INFO

Keywords:
Androstane derivatives
Synthesis
CYP17A1
Androgen receptor
Molecular modeling
Prostate carcinoma cells growth

ABSTRACT

Seven new oxazoline, benzoxazole and benzimidazole derivatives were synthesized from 3β-acetoxyandrosta-5,16-dien-17-carboxylic, 3β-acetoxyandrost-5-en-17β-carboxylic and 3β-acetoxypregn-5-en-21-oic acids. Docking to active site of human 17α-hydroxylase/17,20-lyase revealed that all oxazolines, as well as benzoxazoles and benzimidazoles comprising Δ^{16} could form stable complexes with enzyme, in which steroid moiety is positioned similarly to that of abiraterone and galeterone, and nitrogen atom coordinates heme iron, while 16,17-saturated benzoxazoles and benzimidazoles could only bind in a position where heterocycle is located nearly parallel to heme plane. Modeling of the interaction of new benzoxazole and benzimidazole derivatives with androgen receptor revealed the destabilization of helix 12, constituting activation function 2 (AF2) site, by mentioned compounds, similar to one induced by known antagonist galeterone. The synthesized compounds inhibited growth of prostate carcinoma LNCaP and PC-3 cells at 96 h incubation; the potency of 2′-(3β-hydroxyandrosta-5,16-dien-17-yl)-4′,5′-dihydro-1′,3′-oxazole and 2′-(3β-hydroxyandrosta-5,16-dien-17-yl)-benzimidazole was superior and could inspire further investigations of these compounds as potential anti-cancer agents.

1. Introduction

A number of androstane derivatives modified at C17 with nitrogen containing heterocycles potently and specifically inhibit activity of human cytochrome P450 17α-hydroxylase/17,20-lyase (CYP17A1), and attract attention as potential therapeutic agents for treatment of patients with androgen-dependent cancer [reviews [1–8], and the references therein]. Abiraterone **1** (first-in-class steroidal CYP17A1 inhibitor approved for late-stage prostate cancer) and galeterone **2** (first-in-class multi-target molecule with three reported mechanisms of activity: CYP17A1 inhibition, androgen receptor (AR) antagonism, and induction of AR degradation) are the most studied representatives of that broad class [9–12].

The crystal structures of CYP17A1 complexed with abiraterone **1** and galeterone **2** [13] revealed that nitrogen atom of inhibitor forms a coordinate bond with heme iron, the position of inhibitor in active site is supported by multiple steric and hydrogen bonding features. Molecular dynamics study of CYP17A1 complexes with abiraterone and galeterone [14] provides important insights into the effects of inhibitors on minor structural changes in active site and/or in allosteric site of an enzyme. Investigation of binding mode of galeterone to AR using Induced Fit Docking protocol [15] revealed that orientation of galeterone steroidal nucleus is similar to that of natural androgens, and position of benzimidazole ring is stabilized with accommodation within small hydrophobic pocket, as well as with formation of hydrogen bond between N-3 atom and side chains of Thr877 and Asn705 residues.

Both abiraterone and galeterone inhibited prostate carcinoma cells LNCaP and PC-3 growth and proliferation, and stimulated apoptosis in these cells independently on AR and CYP17A1 activity [16,17]. It was shown that anti-proliferative activities of galeterone and its 3-substituted derivative VNTPT55 against prostate cancer cells caused predominantly by inhibition of oncogenic mRNA translation via antagonizing the Mnk-eIF4E axis [18,19].

Some pyridyl, oxazolinyl, and benzoxazolyl [17(20)*E*]-21-norpregnene derivatives were shown also to be inhibitors of CYP17A1 catalytic activity and prostate carcinoma cells growth [20–24].

* Corresponding author at: N.N. Blokhin Cancer Research Center, Moscow, Russia.
E-mail address: vadimpokrovsky@yandex.ru (V.S. Pokrovsky).

https://doi.org/10.1016/j.steroids.2019.108534
Received 15 June 2019; Received in revised form 1 October 2019; Accepted 25 October 2019
Available online 31 October 2019
0039-128X/

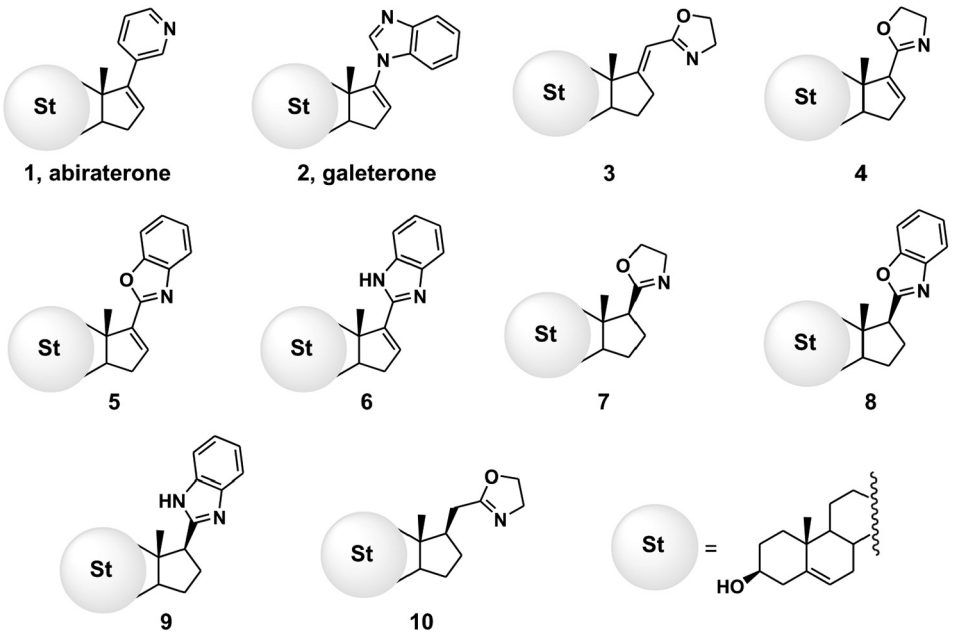

Fig. 1. Structures and chemical names of compounds under investigation: **1**–3′-(3β-hydroxyandrosta-5,16-dien-17-yl)-pyridine; **2** – 1′-(3β-hydroxyandrosta-5,16-dien-17-yl)-(*1H*)-benzimidazole; **3** – [17(*E*)]- 2′-[(3β-hydroxyandrost-5-en-17-ylidene)methyl]-4′,5′-dihydro-1′,3′-oxazole; **4** – 2′-(3β-hydroxyandrosta-5,16-dien-17-yl)-4′,5′-dihydro-1′,3′-oxazole; **5** – 2′-(3β-hydroxyandrosta-5,16-dien-17-yl)-benzo-[*d*]-oxazole; **6** – 2′-(3β-hydroxyandrosta-5,16-dien-17-yl)-(*1H*)-benzimidazole; **7** – 2′-(3β-hydroxyandrost-5-en-17β-yl)-4′,5′-dihydro-1′,3′-oxazole; **8** – 2′-(3β-hydroxyandrost-5-en-17β-yl)-benzo-[*d*]-oxazole; **9** – 2′-(3β-hydroxyandrost-5-en-17-yl)-(*1H*)-benzimidazole; **10** – 2′-[(3β-hydroxyandrost-5-en-17β-yl)methyl]-4′,5′-dihydro-1′,3′-oxazole.

However, structural model of CYP17A1 complex with [17(*E*)]- 2′-[(3β-hydroxyandrost-5-en-17-ylidene)methyl]-4′,5′-dihydro-1′,3′-oxazole **3**, built by molecular dynamic simulations [24], revealed that geometry of this compound makes binding mode with water-bridged heme iron coordination preferential against the mode with direct nitrogen to iron bond, unlike in case with abiraterone **1**, galeterone **2** and other similar androst-16-ene derived inhibitors.

This finding forced us to pay attention on a new azole comprising structures **4 – 10** (Fig. 1). We interested how structural peculiarities of compounds **4 – 10** may affect their interaction with CYP17A1 and AR active sites, and proliferation of prostate carcinoma cells.

In the present study we have synthesized oxazolinyl, benzoxazolyl and benzimidazolyl derivatives of androsta-5,16-diene **4**, **5**, **6**, and their 16,17-saturated analogs **7**, **8**, **9**, as well as oxazoline **10**–17(20)-saturated derivative of previously synthesized compound **3**. New compound **6** is an isomer of galeterone **2**, in which benzimidazole cycle connected to steroid by formation of C2′-C17 bond, rather than N1′-C17 bond found in galeterone. We have also performed docking of compounds **4–10** to CYP17A1 active site, construction of models for androgen receptor ligand binding domain (AR LBD) interaction with compounds **5**, **6**, **8, 9** using molecular dynamic (MD) simulations, and evaluated antiproliferative activity of compounds **4–10** in human prostate carcinoma LNCaP and PC-3 cells in comparison with abiraterone, galeterone and oxazoline **3**.

The data presented below revealed: (i) significant influence of structure of compounds **4–10** on their interaction with CYP17A1, and their effect on AR LBD – most important targets for abiraterone and galeterone; (ii) antiproliferative potency of newly synthesized compounds towards prostate carcinoma LNCaP and PC-3 cells. Among newly synthesized steroidal azoles two compounds: 2′-(3β-hydroxyandrosta-5,16-dien-17-yl)-4′,5′-dihydro-1′,3′-oxazole **4** and 2′-(3β-hydroxyandrosta-5,16-dien-17-yl)-benzimidazole **6** potently suppressed prostate carcinoma cells growth, that could inspire their further investigations as potential anti-cancer agents.

2. Experimental

2.1. Materials and general methods

Melting points were measured in glass capillaries; HRMS were registered on a Bruker 'Apex Ultra' FT ICR MS instrument in ion-positive electrospray ionization mode. ^{1}H NMR and ^{13}C NMR spectra for compounds **11–16** were recorded on AMX-III instrument (Bruker, 400 MHz) in $CDCl_3$ at room temperature (chemical shift of residual solvent protons was 7.25 ppm, of ^{13}C in $CDCl_3$ – 77.2 ppm); ^{1}H NMR and ^{13}C NMR spectra for compounds **4–10** in CD_3OD on Avance III (Bruker, 300 MHz) at 55 °C (chemical shift of residual solvent protons was 3.33 ppm, of ^{13}C in CD_3OD – 47.6 ppm). CD spectra of enantiomerically pure compounds in ethanol were recorded on a 'Jasco-715CD' spectrometer using a quartz cell with 1 cm optical path length (Supplementary data, Fig. S13). Flash chromatography was performed on (0.035–0.070 mm) silica gel from 'Acros', TLC – on Silica gel UV-254 HPTLC plates and UV-254 PTLC plates from 'Merck'. Abiraterone **1** was purchased from 'ChemLeader Ltd' (Shanghai, China), galeterone **2** – from 'Selleck', 2′-{[(*E*)-3β-hydroxyandrost-5-en-17-ylidene]methyl}-4′,5′-dihydro-1′,3′-oxazole **3** was synthesized according the method [23], 3β-acetoxyandrosta-5,16-dien-17-carboxylic acid **11** and 3β-acetoxyandrost-5-en-17β-carboxylic acid **12** were prepared by known methods [25,26], other reagents were purchased from 'Aldrich', 'Merck', and 'Acros'.

2.2. Chemical synthesis

2.2.1. 3β-Acetoxy-21-diazopregn-5-en-20-one 13

Acetylated acid **12** (1.08 g, 3 mmol) was evaporated with dry toluene, then dry toluene (10 mL) was added to the residue, the stirred mixture was cooled to +2 °C, then mixture of oxalyl chloride (1.5 mL, 18 mmol) and dry toluene (10 mL) was added by drops, the mixture was stirred at +2 °C for 10 min, thereafter the solution obtained was kept for 2 h at room temperature. The mixture was repeatedly evaporated with dry toluene, and the resulted acyl chloride **12a** was dissolved in dry toluene (10 mL). The excess of ethereal solution of diazomethane was added to the acyl chloride solution, the mixture was stirred at room temperature for 1 h, and then evaporated to dryness. The residue was twice crystallized from hexane to obtain diazoketone **13** (770 mg, 2.0 mmol, 67%) as slightly yellow needles with m. p. 141 °C. HRMS, calculated for $[C_{23}H_{33}N_2O_3]^+$: 385.2491; found: 385.2487; ^{1}H NMR ($CDCl_3$): 0.69 (3H, s, H-18); 1.02 (3H, s, H-19); 2.02 (3H, s, Ac); 4.60 (1H, m, H-3); 5.16 (br. s, CHN_2); 5.36 (1H, m, H-6); ^{13}C NMR ($CDCl_3$): 13.2, 19.3, 20.9, 21.4, 23.0, 24.5, 27.7, 31.8, 31.9, 36.6, 37.0, 38.1, 38,6, 44.8, 50.2, 54.8, 56.7, 61.4, 73.8, 122.3, 139.7, 170.5, 195.0.

2.2.2. 3β-Acetoxypregn-5-en-21-oic acid 14

Mixture of compound **13** (576 mg, 1.5 mmol), dioxane (10 mL), water (5 mL) and CH_3COOAg (10 mg, 0.06 mmol) was stirred at 70 °C for 1 h, and thereafter evaporated to dryness. The residue was treated with $CHCl_3$ (30 mL) and 5% aqueous CH_3COOH (10 mL), aqueous layer was washed with $CHCl_3$ (2 × 10 mL), the combined chloroform extract was washed with brine, dried over Na_2SO_4, evaporated, the residue was crystallized from CH_3CN to obtain acid **10** (485 mg, 1.3 mmol, 87%) as white cubes with m. p. 146 °C. HRMS, calculated for $[C_{23}H_{35}O_4]^+$: 375.2530; found: 375.2541; ^{1}H NMR ($CDCl_3$): 0.61 (3H, s, H-18); 1.02 (3H, s, H-19); 2.02 (3H, s, Ac) 4.59 (1H, m, H-3); 5.36 (1H, m, H-6); ^{13}C NMR ($CDCl_3$): 12.4, 19.3, 20.8, 21.4, 24.6, 27.8, 28.2, 31.9 (x2), 34.8, 36.7, 37.0, 37.2, 38.1, 42.0, 46.6, 50.2, 55.5, 73.9, 122.5, 139.7, 170.6, 179.1.

2.2.3. Procedure for preparation of oxazolines 4, 7, 10

Acetylated acid (**11**, **12**, or **14,** 1 mmol) was evaporated with dry pyridine, then mixture of obtained pyridinium salt, triphenyl phosphine (1.0 g, 3.8 mmol) and dry CH_3CN (10 mL) was cooled to + 2 °C under constant stirring; then mixture of CCl_4 (0.97 mL, 10 mmol) and dry CH_3CN (5 mL) was added by drops during 10 min at + 2 °C, and the mixture was stirred by cooling for 90 min, until clear solution formed. After that, solution of ethanolamine (80 μL, 1.3 mmol) and triethyl amine (557 μL, 4 mmol) in 5 mL of dry CH_3CN was added by drops during 10 min at +2 °C, and mixture was stirred at +2 °C for 10 min more. Then, ice bath was removed, and the mixture was kept stirring at ambient temperature for 2 h, until intermediately formed amide disappeared completely. The solution was concentrated to the volume of 5 mL, diluted with benzene (30 mL). Resulting solution was washed with saturated K_2CO_3 solution (10 mL), then with brine (20 mL), dried over Na_2SO_4 and evaporated. The residue was dissolved in 9 mL of boiled toluene, diluted with 12 mL of boiled hexane and stored for 2 h at room temperature. Resulted crystalline triphenyl phosphine oxide was filtered off, washed with cold toluene–hexane mixture (3:4), the combined filtrate was evaporated and the residue was subjected to silica gel flash chromatography in hexane–acetone (2:1) mixture to give 3β-acetylated oxazoline. Obtained acetate was dissolved in methanol (5 mL), then water (3 mL) and K_2CO_3 (1.0 g) were added, the mixture was stirred and heated under reflux for 40 min, cooled, treated with $CHCl_3$ (20 mL) and water (5 mL), the aqueous layer was extracted with $CHCl_3$ (15 mL); combined chloroform extract was washed with brine (20 mL), dried over Na_2SO_4, evaporated, and target oxazoline was purified by silica gel flash chromatograpy in hexane–acetone (3:2) mixture, followed by crystallization from appropriate solvent.

2.2.4. 2′-(3β-Hydroxyandrosta-5,16-dien-17-yl)-4′,5′-dihydro-1′,3′-oxazole 4

Oxazoline **4** (185 mg, 0.54 mmol, 54% based on starting **11**); white needles, m. p. 165 °C (from acetone). HRMS, calculated for $[C_{22}H_{32}NO_2]^+$: 342.2428; found: 342.2419; ^{1}H NMR (CD_3OD): 0.99 (3H, s, H-18); 1.09 (3H, s, H-19); 3.42 (1H, m, H-3); 3.89 and 4.25 (each 2H, m, CH_2-oxazoline); 5.38 (1H, m, H-6); 6.54 (1H, dd, J = 2.0 Hz, J = 3.2 Hz H-16) ^{13}C NMR (CD_3OD): 14.9 (C-18); 18.4 (C-19); 20.5 (C-11); 30.4 (C-8); 30.9 (C-2); 31.2 (C-7); 31.4 (C-15); 34.8 (C-12); 36.5 (C-10); 37.1 (C-1); 41.7 (C-4); 46.1 (C-13); 50.8 (C-9); 53.9 (C-5′); 57.0 (C-14); 66.0 (C-4′); 71.0 (C-3); 120.6 (C-6); 138.8 (C-16); 141.4 (C-5); 143.0 (C-17); 162.8 (C-2′).

2.2.5. 2′-(3β-Hydroxyandrost-5-en-17β-yl)-4′,5′-dihydro-1′,3′-oxazole 7

Oxazoline **7** (151 mg, 0.44 mmol, 44% based on starting **12**); white needles, m. p. 181 °C (from acetone). HRMS, calculated for $[C_{22}H_{34}NO_2]^+$: 344.2584; found: 344.2569; ^{1}H NMR (CD_3OD): 0.72 (3H, s, H-18); 1.05 (3H, s, H-19); 3.42 (1H, m, H-3); 3.78 and 4.28 (each 2H, m, CH_2-oxazoline); 5.36 (1H, m, H-6); ^{13}C NMR (CD_3OD): 12.1 (C-18); 18.4 (C-19); 20.7 (C-11); 24.1 (x2) (C-15, C-16); 30.9 (C-2); 31.5 (C-7); 32.1 (C-8); 36.4 (C-10); 37.2 (C-1); 38.0 (C-1); 41.7 (C-4); 43.7 (C-13); 49.5 (C-17); 50.4 (C-9); 52.9 (C-5′); 56.0 (C-14); 66.9 (C-4′); 71.0 (C-3); 120.7 (C-6); 141.1 (C-5); 170.7 (C-2′).

2.2.6. 2′-[(3β-Hydroxyandrost-5-en-17β-yl)methyl]-4′,5′-dihydro-1′,3′-oxazole 10

Oxazoline **10** (186 mg, 0.52 mmol, 52% based on starting **14**); white needles, m. p. 172 °C (from methanol). HRMS, calculated for $[C_{23}H_{36}NO_2]^+$: 358.2741; found: 358.2741; ^{1}H NMR (CD_3OD): 0.70 (3H, s, H-18); 1.05 (3H, s, H-19); 3.42 (1H, m, H-3); 3.77 and 4.28 (each 2H, m, CH_2-oxazoline); 5.36 (1H, m, H-6); ^{13}C NMR (CD_3OD): 11.1 (C-18); 18.5 (C-19); 20.6 (C-11); 24.1 (C-15); 27.8 (C-16); 28.1 (C-20); 31.0 (C-2); 31.6 (C-7); 32.0 (C-8); 36.4 (C-10); 37.1 (C-1); 37.2 (C-12); 41.7 (C-4); 41.8 (C-13); 47.5 (C-17); 50.7 (C-9); 53.0 (C-5′); 55.9 (C-14); 67.3 (C-4′); 71.1 (C-3); 120.8 (C-6); 141.1 (C-4); 170.7 (C-2′).

2.2.7. Procedure for preparation of benzoxazoles 5, 8

Stirred mixture of carboxylic acid (**11**, **12**, 0.5 mmol), triphenyl phosphine (524 mg, 2 mmol), dry pyridine (3 mL) and dry CH_3CN (3 mL) was cooled to + 2 °C, then mixture of CCl_4 (483 μL, 5 mmol) and dry CH_3CN (1 mL) was added by drops at + 2 °C. Resulting mixture was stirred at +2 °C for 90 min, until clear solution formed. Solution of o-aminophenol (71 mg, 0.65 mmol) and dry pyridine (200 μL, 2.5 mmol) in 1 mL of dry CH_3CN was added by drops at +2 °C, and the mixture was stirred at +2 °C for 10 min, then at 20 °C for 20 min more. Triphenyl phosphine (262 mg, 1 mmol) was added, and the mixture was stirred at 50 °C for 3 h, until amide disappeared completely. The mixture was concentrated by evaporation, the residue was dissolved in benzene (25 mL), treated with $NaHCO_3$ saturated solution (10 mL), upper layer was washed with brine (10 mL), dried over Na_2SO_4, evaporated to dryness. The residue was dissolved in 9 mL of boiled toluene, diluted with 12 mL of boiled hexane and stored for 2 h at room temperature. Resulted crystalline triphenyl phosphine oxide was filtered off, washed with cold toluene–hexane mixture (3:4), the combined filtrate was evaporated and the residue was subjected to silica gel flash chromatography in hexane–acetone (2:1) mixture to give 3β-acetylated benzoxazole. Obtained acetate was dissolved in methanol (5 mL), then water (3 mL) and K_2CO_3 (1.0 g) were added, the mixture was stirred and heated under reflux for 40 min, cooled, treated with $CHCl_3$ (20 mL) and water (5 mL), aqueous layer was extracted with $CHCl_3$ – methanol mixture (2:1, 15 mL); combined extract was washed with brine (20 mL), dried over Na_2SO_4, evaporated, and target benzoxazole was purified by silica gel flash chromatograpy in hexane–acetone (3:2) mixture.

2.2.8. 2′-(3β-Hydroxyandrosta-5,16-dien-17-yl)-benzo-[d]-oxazole 5

Benzoxazole **5** (156 mg, 0.4 mmol, 40% based on starting **11**); light beige needles, m. p. 173 °C (from methanol). HRMS, calculated for $[C_{26}H_{32}NO_2]^+$: 390.2428; found: 390.2422; ^{1}H NMR (CD3OD): 1.12 and 1.13 (each 3H, s, H-18, H-19); 3.43 (1H, m, H-3); 5.39 (1H, m, H-6); 6.91 (1H, dd, J = 2.0 Hz, J = 3.3 Hz), 7.34 (2H, m, aromatic); 7.50–7.75 (2H, m, aromatic); ^{13}C NMR (CD_3OD): 15.1 (C-19); 18.4 (C-18); 20.6 (C-11); 30.4 (C-8); 31.0 (C-2); 31.2 (C-7); 31.9 (C-15); 34.9 (C-12); 36.4 (C-10); 37.1 (C-1); 41.7 (C-4); 46.6 (C-13); 50.8 (C-9); 57.0 (C-14); 71.0 (C-3); 109.9 (C-5′); 119.2 (C-8′); 120.5 (C-6); 124.5 (C-6′); 124.9 (C-7′); 138.8 (C-16); 141.5 (x2) (C-5, C-4′)); 142.4 (C-17); 149.9 (C-9′); 168.0 (C-2′).

2.2.9. 2-(3β-Hydroxyandrost-5-en-17-yl)-benzo-[d]-oxazole 8

Benzoxazole **8** (166 mg, 0.42 mmol, 42% based on starting **12**); milky white needles, m. p. 215 °C (from methanol). HRMS, calculated for $[C_{26}H_{34}NO_2]^+$: 392.2584; found: 392.2577; ^{1}H NMR (CD3OD): 0.66 (3H, s, H-18); 1.05 (3H, s, H-19); 3.03 (1H, m, H-17); 3.44 (1H, m, H-3); 5.39 (1H, m, H-6); 7.35 (2H, m, aromatic); 7.50–7.75 (2H, m, aromatic); ^{13}C NMR (CD_3OD): 12.4 (C-18); 18.4 (C-19); 20.7 (C-11); 24.2 (C-15); 24.5 (C-16); 31.0 (C-2); 31.5 (C-7), 32.2 (C-8); 36.4 (C-10); 37.2 (C-1); 37.9 (C-12); 41.7 (C-4); 45.2 (C-13); 50.2 (C-17); 50.4 (C-9); 56.1 (C-14); 71.0 (C-3); 109.9 (C-5′); 118.6 (C-8′); 120.7 (C-6); 124.0

(C-6′); 124.5 (C-7′); 140.5 (C-4′); 141.1 (C-5); 150.7 (C-9′); 168.6 (C-2′).

2.2.10. Procedure for preparation of amides 15, 16

Acetylated acid (**11**, or **12**, 1 mmol) was evaporated with dry toluene, then dry toluene (5 mL) was added to the residue, the stirred mixture was cooled to + 2 °C, then solution of oxalyl chloride (0.5 mL, 6 mmol) in dry toluene (5 mL) was added by drops, the mixture was stirred at +2 °C for 10 min, thereafter the solution obtained was kept for 2 h at room temperature. The mixture was repeatedly evaporated with dry toluene, and resulted acyl chloride (**11a,** or **12a**) was dissolved in dry toluene (5 mL). The solution obtained was added by drops to the cooled solution of *o*-phenylene diamine (152 mg, 1.4 mmol) and triethyl amine (160 μL, 2.0 mmol) in dry dichloromethane (3 mL), the mixture was stirred for 1 h, evaporated, and the residue was treated with $CHCl_3$ (20 mL) and $NaHCO_3$ saturated solution (10 mL). Chloroform extract was washed with 1% HCl (2 × 5 mL), brine (2 × 5 mL), dried over Na_2SO_4 and evaporated to dryness to obtain crude amide (**15**, or **16**) in near quantitative yield as slightly yellow solid foam, which was used further purification. The crude amide **15** contained impurity – 1,2-*bis*(3β-acetoxyandrosta-5,16-dien-17-yl)carbamoyl]-phenylene **15a** (7%), the crude amide **16** – 1,2-*bis*-(3β-acetoxyandrost-5-en-17-yl)carbamoyl]-phenylene **16a** (10%). Analytical samples of compounds **15, 15a**, **16**, and **16a** were obtained by TLC of crude amides in hexane–acetone-ethyl acetate (3:1:1) mixture.

2.2.11. 3β-Acetoxy-17-(2-aminophenylcarbamoyl)androsta-5,16-diene 15

Amide **15**; HRMS, calculated for $[C_{28}H_{37}N_2O_3]^+$: 449.2799; found: 449.2792; ^{1}H NMR ($CDCl_3$): 1.06; 1.08 (each 3H, s, H-18 and H-19); 2.03 (3H, s, Ac); 4.59 (1H, m, H-3); 5.38 (1H, m, H-6); 6.49 (1H, m, H-16); 6.70–6.84 (2H, m, aromatic); 7.04 (2H, m, aromatic); 7.30 (1H, m, aromatic); ^{13}C NMR ($CDCl_3$): 16.4, 19.2, 20.7, 21.4, 27.7, 30.2, 31.5, 32.0, 34.7, 36.9, 38.1, 46.7, 50.4, 56.6, 73.8, 118.3, 119.7, 122.0, 124.9, 126.8, 128.0, 130.6, 137.0, 137.2, 140.2, 140.4, 164.6, 170.5.

2.2.12. 1,2-bis-[(3β-Acetoxyandrosta-5,16-dien-17-yl)carbamoyl]-phenylene 15a

Bis-amide **15a**; HRMS, calculated for $[C_{50}H_{65}N_2O_6]^+$: 789.4837; found: 789.4821; ^{1}H NMR ($CDCl_3$): 1.05 and 1.06 (each 6H, s, H-18 and H-19); 2.02 (6H, s, Ac); 4.60 (2H, m, H-3); 5.38 (2H, m, H-6); 6.49 (2H, m, H-16); 7.16 and 7.45 (each 2H, m, aromatic); 8.17 (2H, br. s, NH); ^{13}C NMR ($CDCl_3$): 13.3, 19.3, 21.0, 21.4, 23.9, 24.6, 27.7, 31.8, 31.9, 36.7, 37.1, 38.1, 38.5, 44.3, 56.4, 57.6, 72.8, 122.3, 125.4, 126.0, 130.7, 139.8, 170.5, 172.2.

2.2.13. 3β-Acetoxy-17-(2-aminophenylcarbamoyl)androst-5-ene 16

Amide **16**; HRMS, calculated for $[C_{28}H_{39}N_2O_3]^+$: 451.2955; found: 451.2950; ^{1}H NMR ($CDCl_3$): 0.80 (3H, s, H-18); 1.02 (3H, s, H-19); 2.02 (3H, s, Ac); 4.60 (1H, m, H-3); 5.38 (1H, m, H-6); 6.77 and 7.03 (each 2H, m, aromatic); 7.16 (1H, m, aromatic); ^{13}C NMR ($CDCl_3$): 13.3, 19.3, 21.0, 21.4, 23.8, 24.6, 27.7, 31.8, 31.9, 36.7, 37.1, 38.1, 38.5, 44.2, 50.0, 56.5, 57.5, 73.9, 118.3, 119.5, 122.3, 125.1, 124.8, 127.0, 139.7, 140.8, 170.5, 171.5.

2.2.14. 1,2-bis-[(3β-Acetoxyandrost-5-en-17-yl)carbamoyl]-phenylene 16a

Bis-amide **16a**; HRMS, calculated for $[C_{50}H_{69}N_2O_6]^+$: 793.5150; found: 793.5135; ^{1}H NMR ($CDCl_3$): 0.79 (6H, s, H-18); 1.03 (6H, s, H-19); 2.02 (6H, s, Ac); 4.60 (2H, m, H-3); 5.39 (2H, m, H-6); 7.14 and 7.41(each 2H, m, aromatic); 7.84 (2H, br. s, NH); ^{13}C NMR ($CDCl_3$): 13.3, 19.3, 21.0, 21.4, 23.9, 24.6, 27.7, 31.8, 31.9, 36.7, 37.1, 38.1, 38.5, 44.3, 50.0, 56.4, 57.6, 72.8, 122.3, 125.4 (x2), 126.0 (x2), 130.7, 139.8, 170.5, 172.2.

2.2.15. Procedure for preparation of benzimidazoles 6, 9

Solution of crude amide (15, or 16, 0.5 mmol) in 8 mL of dry toluene was placed in 50-mL round bottom flask, then acid Al_2O_3 (100 mg) was added to this solution, thereafter the mixture was rotary evaporated to dryness. The flask, containing residue as solid film, was placed in a microwave oven 'Samsung ME83KRS-2′ and exposed to irradiation at 700 W for 10 min. After cooling, triethyl amine (100 μL), $CHCl_3$ (5 mL), and SiO_2 (1.5 g) were added to the residue, the mixture was evaporated to dryness, the residue was applied on the top of short column filled with silica gel, and acetylated benzimidazole was eluted with hexane–acetone (2:1) mixture, followed by evaporation. Mixture of the acetate obtained, methanol (5 mL), water (3 mL) and K_2CO_3 (1.0 g) was stirred and heated under reflux for 40 min, cooled, treated with $CHCl_3$ (20 mL) and water (5 mL), aqueous layer was extracted with $CHCl_3$ – methanol mixture (2:1, 15 mL); combined extract was washed with brine (20 mL), dried over Na_2SO_4, evaporated, purified by preparative TLC in hexane–acetone (2:1) mixture, followed by crystallization from methanol.

2.2.16. 2′-(3β-Hydroxyandrosta-5,16-dien-17-yl)-(1H)-benzimidazole 6

Benzimidazole **6** (130 mg, 0.34 mmol, 67% based on starting **11**); white needles, m. p. 190C (from methanol). HRMS, calculated for $[C_{26}H_{33}N_2O]^+$: 389.2587; found: 359.2580; ^{1}H NMR (CD_3OD): 1.13 (3H, s, H-18); 1.18 (3H, s, H-19); 3.45 (1H, m, H-3); 5.40 (1H, m, H-6); 6.59 (1H, dd, J = 1.9 Hz, J = 3.3 Hz, H-16), 7.21 and 7.35 (each 2H, m, aromatic); ^{13}C NMR (CD_3OD): 15.2 (C-18); 18.4 (C-19); 20.6 (C-11); 30.4 (C-8); 31.0 (C-2); 31.3 (C-7); 31.6 (C-15); 34.9 (C-12); 36.6 (C-10); 37.1 (C-1); 41.7 (C-4); 46.7 (C-13); 50.9 (C-9); 57.4 (C-14); 71.1 (C-3); 114.3 (x2) (C5′, C8′); 120.6 (C-6); 122.0 (x2) (C-6′, C-7′); 133.6 (C-16); 141.4, (C-5); 145.3 (C-17), 149.3 (x2) (C-4′, C-9′); 159.2 (C-2′).

2.2.17. 2′-(3β-Hydroxyandrost-5-en-17-yl)-(1H)-benzimidazole 9

Benzimidazole **9** (125 mg, 0.32 mmol, 64% based on starting **12**); white needles, m. p. 210C (from methanol). HRMS, calculated for $[C_{26}H_{35}N_2O]^+$: 391.2744; found: 391.2741; ^{1}H NMR (CD_3OD): 0.65 (3H, s, H-18); 1.04 (3H, s, H-19); 2.98 (1H, t, J = 9.9 Hz, H-17) 3.44 (1H, m, H-3); 5.38 (1H, m, H-6); 7.19 and 7.52 (each 2H, m, aromatic); ^{13}C NMR (CD_3OD): 12.4 (C-18); 18.4 (C-19); 20.7 (C-11); 24.2 (C-15); 25.0 (C-16); 30.9 (C-2); 31.6 (C-7); 32.3 (C-8); 36.4 (C-10); 37.2 (C-1); 37.7 (C-12); 41.7 (C-4); 44.9 (C-13); 50.5 (C-9); 50.8 (C-17); 56.2 (C-14); 71.1 (C-3); 113.9 (x2) (C-5′, C-8′); 120.8 (C-6); 121.7(×2) (C-6′, C-7′); 137.9 (x2) (C-4′, C-9′); 141.1 (C-5); 155.4 (C-2′).

2.3. Molecular modeling

2.3.1. Docking of compounds 4–10 to CYP17A1 active site

The structure of cytochrome P450 17A1 in complex with abiraterone, obtained from the protein data bank (code 3RUK) was used for docking. Structures of compounds **4 – 10** were generated using SYBYL 8.1 program (Tripos Inc.). Structures of the tested compounds and protein were optimized by Powell's method of energy minimization using Tripos force field in vacuum. The partial atomic charges for the protein and tested compounds were calculated by Gasteiger-Huckel method.

Docking was carried out using Vina Autodock package [34], and non-ring single bonds of the ligand were allowed to rotate. The ligand poses obtained from docking calculations were ranked and chosen based on its binding energies and geometrical properties. To evaluate the correctness of poses of the docked molecules, ligand positions from crystal structures were used as a reference template. Analysis of intermolecular interactions between protein and docked molecules was performed using PLIP server [44].

2.3.2. MD modeling of compounds 2, 5, 6, 8, 9 interaction with AR LBD

Crystal structure of AR LBD in complex with testosterone (PDB code 2AM9) was used as starting point for simulations. Initial structure was placed into dodecahedral unit cell for use with periodic boundary conditions (cell parameters $a = b = c = 70$ Å), solvated with TIP3P water [27] and ionized with NaCl to 0.15 M. The system was minimized

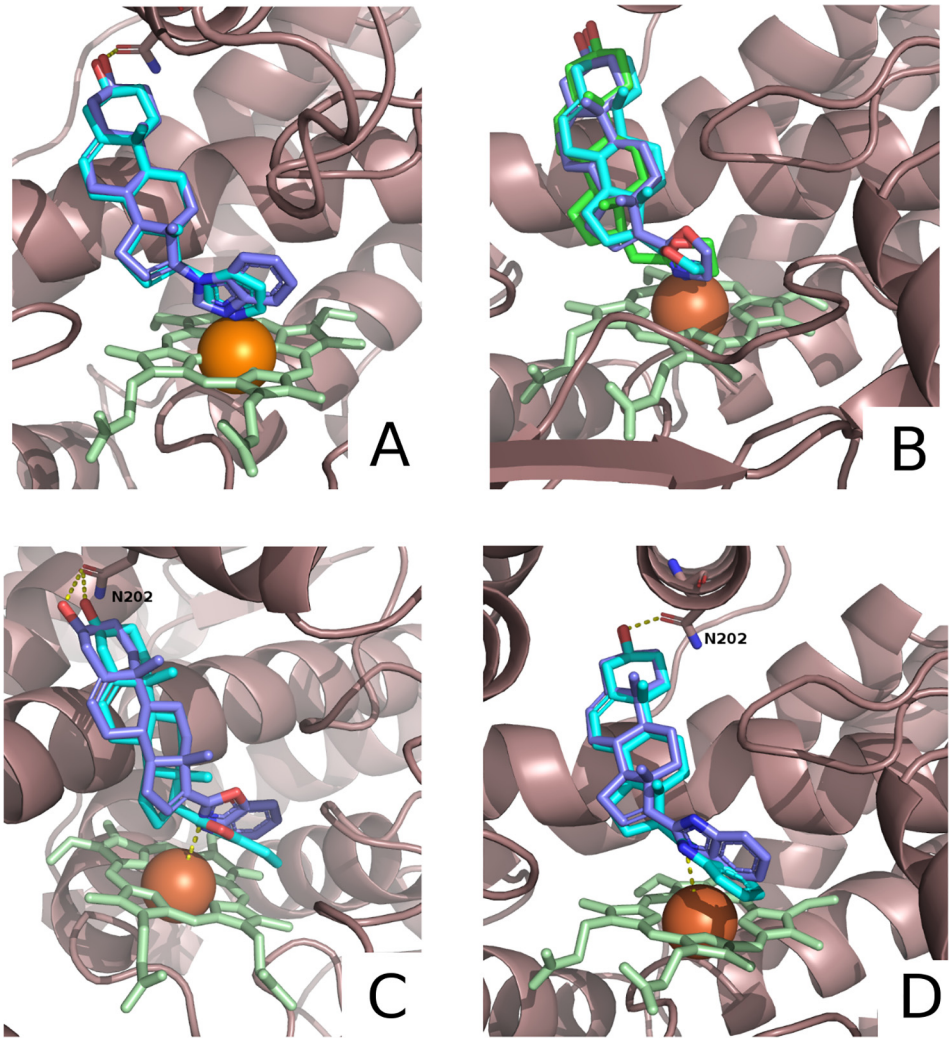

Fig. 2. Docking of compounds under investigation to CYP17A1 active site. A – docking poses for abiraterone **1** (cyan, ΔH = -9.3 kcal/mol) and galeterone **2** (blue, ΔH = −12.9 kcal/mol); B – docking poses for oxazolines **4** (blue, ΔH = -9.3 kcal/mol), **7** (cyan, ΔH = −9.2 kcal/mol) and **10** (green, ΔH = -8.5 kcal/mol); C – docking poses for benzoxazoles **5** (blue, ΔH = −10.5 kcal/mol) and **8** (cyan, ΔH = -8.2 kcal/mol); D – docking poses for benzimidazoles **6** (blue, ΔH = −10.7 kcal/mol) and **9** (cyan, ΔH = −8.3 kcal/mol).

for 5000 steps using steepest descent minimizer, then equilibrated with 2 fs time step for 50,000 steps in NVT regime using Berendsen thermostat, followed by NPT equilibration for 500,000 steps. Protein heavy atoms were constrained during equilibration. For the production run of 200 ns length, NPT ensemble was simulated by using Nose-Hoover temperature coupling [28] and isotropic Parrinello-Rahman pressure coupling method [29]. Temperature during simulation was 310 K. Data frames were recorded every 10 ps. To avoid non-equilibrium effects, the initial 60 ns were not used in analysis. Equilibration was assessed by protein RMSD plot (Fig. S9-1), and residue-wise backbone RMSF stayed below 1 Å besides few loop regions (Fig. S9-2). Trajectories for AR LBD complexes with galeterone **2** and compounds **5**, **6**, **8**, **9** were calculated using the same method.

All simulations were performed with full-atom CHARMM36 force field [30], using GROMACS software [31] on 6-core 3.50 GHz Intel(R) Xeon(R) CPU E5-1650 v3 workstation equipped with dual Quadro K2200 GPUs (Nvidia). CHARMM parameters for ligands were obtained from Swiss-Param server [32]. VMD [33] was used for MD trajectory analysis and visualization. For docking, AutoDock Vina [35] was used along with custom scripts to run docking jobs in batch.

2.4. Cell cultures and cell growth analysis

Human prostate carcinoma cells LNCaP and PC-3 were obtained from the American Type Culture Collection (Rockville, MD). Cells were propagated in culture dishes at the desired densities in RPMI 1640 medium supplemented with 10% fetal calf serum (FCS; Gibco, Grand Island, NY), and 1% penicillin/streptomycin (Gibco) in a 5% CO2 atmosphere at 37 °C for 24 h. The cells were seeded at 2×10^4 cells/well for 48 h, then treated with tested compounds at the designated concentrations, and incubated for an additional 96 h.

Effect of compounds on cell growth was examined by MTT assay [36]. Solution of 3-(4,5-dimethylthiazol-2-yl)-2,5-diphenyltetrazolium bromide (MTT, 5 mg/mL) was added, and cells were incubated for 4 h, followed by absorbance measurement at 570 nm, with 'SpectraMax 190′ microplate reader. Viability of treated cells was expressed as a percentage relative to control. Each experiment was performed in triplicate, and independently repeated at least four times. We used Hill model to fit dose response curve considering Hill slope to be equal 1 [37]. GI_{50} was estimated as one of the parameters of Hill equation. Data analysis was performed using SPSS 21 and R software packages. Statistical significance of differences between discussed compound activities was assessed by pair-wise ANOVA.nls [38] method, using p-value cutoff of 0.05.

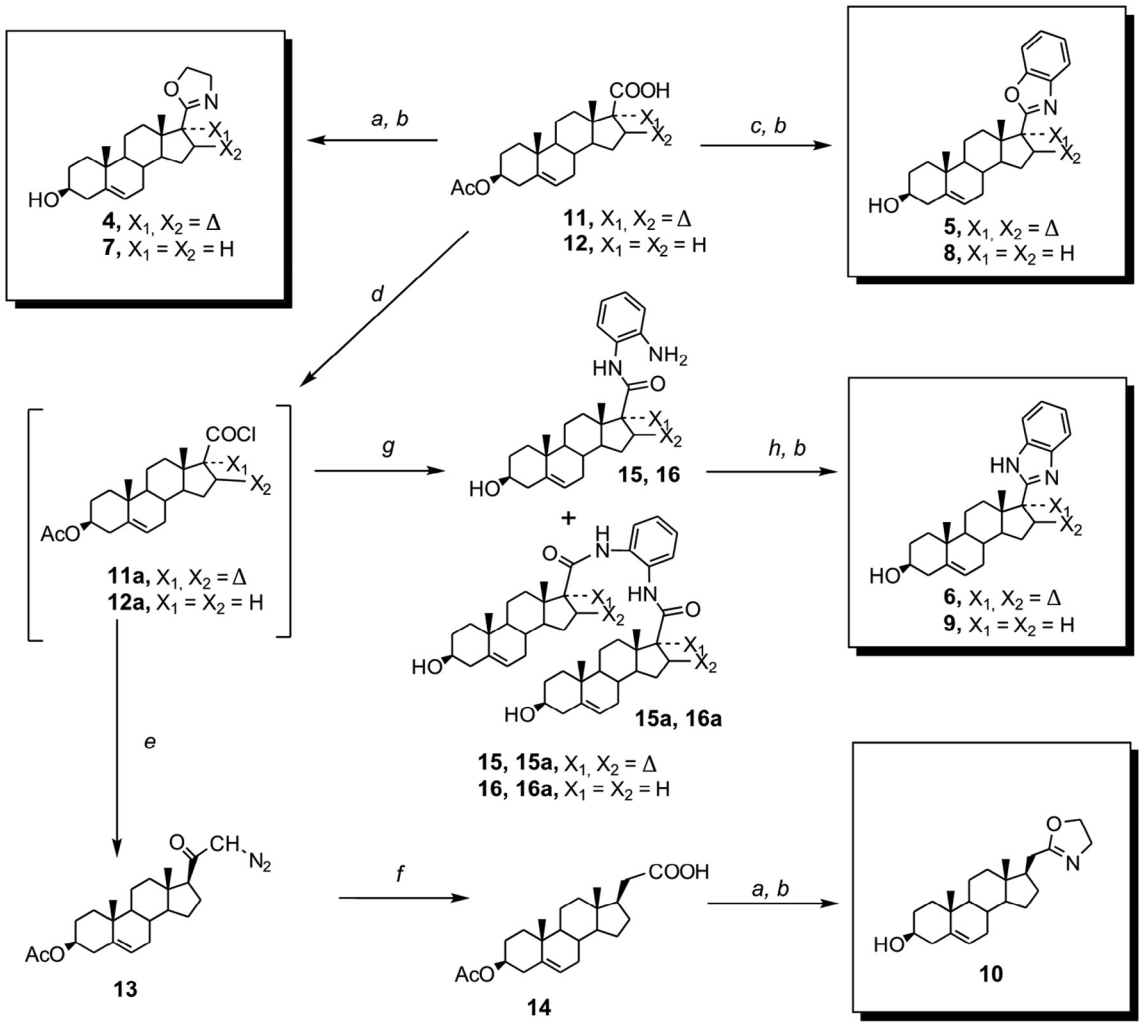

Scheme 1. *a* – Ph_3P, CCl_4 / CH_3CN, +2°C, 2 h, then $NH_2(CH_2)_2OH$, Et_3N / CH_3CN, +2°C → r. t., 2 h; *b* – K_2CO_3 / MeOH - H_2O, Δ, 40 min; *c* – Ph_3P, CCl_4 / CH_3CN, pyridine + 2 °C, 2 h, then *o*-$NH_2(C_6H_4)OH$, pyridine/ CH_3CN, +50 °C, 3 h; *d* – $(COCl)_2$ / toluene, +2°C → r. t., 2 h; *e* – CH_2N_2, r. t., 1 h; *f* – H_2O, dioxane, Ag+, 70 °C, 1 h; *g* – *o*-$NH_2(C_6H_4)NH_2$, Et_3N/ CH_2Cl_2, r. t., 1 h; *h* – Al_2O_3, MW irradiation.

3. Results and discussion

3.1. Chemical synthesis

Simple synthesis of target compounds **4–10** is presented on the Scheme 1. Transformation of acetylated acid **12** to related homologous acid **14** was performed by Arndt - Eistert reaction [39]**:** compound **12** was treated with oxalyl chloride, then resulting acyl chloride **12a**, without isolation step, was treated with an excess of diazomethane to obtain diazoketone **13**, which rearranged into acid **14** under heating with aqueous dioxane in the presence of Ag^+ ions.

3β-Acetylated acids **11**, **12** and **14** were transformed to oxazolines **4**, **7**, **10** according to the procedure [23]; acids **11** and **12** – to benzoxazoles **5** and **8** according to the procedure [24]. Our attempts to obtain benzimidazoles **6** and **9** from steroidal acids **11** and **12** with *o*-phenylene diamine and acid catalyst (either in the absence, or in the presence of microwave irradiation [40,41]), were slightly successful.

For preparation of benzimidazoles **6** and **9,** acetylated acids **11** and **12** were initially transformed to related acyl chlorides **11a** and **12a**, then treated with *o*-phenylene diamine, leading to amides **15** and **16** (containing admixtures of *bis*-amides **15a** and **16a**). Cyclization of crude amides **15** and **16** under microwave irradiation in the presence of Al_2O_3, followed by removal of acetate protective groups, led to target benzimidazoles **6** and **9** in overall 67% and 64% yields (calculated on starting acids **11** and **12**, respectively).

3.2. Molecular modeling

Structures of oxazolines **4**, **7** and **10** were successfully docked to the crystal structure of CYP17A1 (PDB id 3RUK). Control docking of abiraterone **1** and galeterone **2** reproduced the protein–ligand complex with 0.51 Å RMSD (Fig. 2A).

Detailed binding mode analysis showed that oxazoline cycles of compounds **4, 7** and **10** were positioned in the vicinity of heme plane in such a way for heme iron to be able to form coordination bond with oxazoline nitrogen; steroid moieties of all the compounds were positioned similarly; 3β-hydroxyl groups of all compounds were found in close proximity of Asn-202 in the F helix, which allows the formation of corresponding hydrogen bonds (Fig. 2B). Positions of oxazolines **4, 7** and **10** in the active site of CYP17A1 were close to that of abiraterone **1** (Fig. 2A), and different from that for [17(20)*E*]-21-norpregnene oxazoline **3** [24].

Docking of benzoxazoles **5** and **8** (Fig. 2C) and benzimidazoles **6** and **9** (Fig. 2D) demonstrated that compounds **5** and **6** (comprising Δ^{16}) could form stable complexes with CYP17A1 resembling complex CYP17A1 – galeterone **2** (Fig. 2A), in which nitrogen atom coordinates with heme iron, while compounds **8** and **9** (comprising saturated 16,17-bond) can only be positioned in the active site in such a way that

heterocycle is nearly parallel to the heme plane. Results of our docking studies are in agreement with published investigation of steroidal CYP17A1 inhibitors [42], and suggests possible high inhibitory potency for compounds **4 – 10**, particularly for oxazoline **4**.

Published data [10–12] shows that abiraterone and related 3β-hydroxyandrosta-5,16-dienes modified at C17 with 5- or 6-member nitrogen containing heterocycle possessed rather weak affinity to AR, therefore, we focused on modeling of AR LBD interaction with galeterone **2** and its analogs, compounds **5, 6, 8, 9**. Our attempts to dock them directly into 2AM9 crystal structure of AR LBD did not succeed. This is expected, as the galeterone, possessing anti-androgen activity, presumably cannot bind in the way identical to androgens, such as testosterone and dihydrotestosterone. However, removal of Helix 12 from AR LBD structure allows docking of potential ligands in the similar manner (Supplementary data, Fig. S8). This incomplete receptor structure differs in the absence of bulky residues located near position 17 in testosterone, and taking into account large 17-substituent of galeterone, it is clear that steric clash in that region prevents construction of models by docking into intact 2AM9 structure. However, previous modeling efforts show that, allowing the change in conformation of the amino acid residues side chains lining the binding site lead to possibility of galeterone accommodation in the active site of AR LBD [15].

Molecular Dynamics (MD) simulations provides the most accurate way to reproduce protein side chain flexibility, and we used it to construct the models of intact AR LBD complexes with galeterone **2** and compounds **5, 6, 8, 9**. Trajectory of 200 ns length was calculated, with explicit water, for the complex of AR LBD with testosterone. Then, docking was performed, in automatic manner, into each frame of the resulting trajectory, to identify conformations of the binding site suitable to accommodate the ligands, and docking energy score and position of steroid skeleton were used as the criteria for selection of preferred ligand binding poses.

Conformations with docking energy of more than 4 kcal/mol above the best one were discarded, and the resulting sets were clustered using DBSCAN algorithm, according to their orientation relative to the protein, and the dihedral angle determining the position of 17-substituent relative to the steroid skeleton. Docking poses for compounds **5**, **6**, **8**, **9** with the lowest energy found in clusters with RMSD of the steroid skeleton close to one in 2AM9 are shown on Fig. 3 (A, B; corresponding clusters – on Fig. S10). It can be seen that bulky 17-substutuent positioned underneath the H12 helix, the rotation of which is considered to be the mechanism of antagonistic action towards AR [42].

In crystal structure 2AM9, used as starting point for MD simulation, Arg752 side chain is folded inside the channel near Gln711 and 3-keto oxygen of testosterone. In the very beginning of MD simulation, however, Arg752 side chain moves outside the binding site and becomes completely exposed to the water. That “outside” Arg752 side chain conformation is further stabilized by the possibility of salt bridge formation with Glu681 on the surface of the protein. As the result, much more freedom opens for steroid displacement in direction parallel to its long axis, which presumably renders ligand binding site of AR to be ready to accommodate molecules with bulkier substituent at 17 position.

However, inhibitor binding must clearly lead to more drastic global conformation changes in the LBD, with most commonly accepted model being helix 12 (H12) rotation [42,43]. In course of our simulation, the backbone atoms of residues which constitute the binding site did not move a lot (Fig. S8-5, red circles), and H12 also fluctuated very moderately. Therefore, modes of antagonist binding obtained by docking are still far from equilibrium, and we performed additional 300 ns of MD in order to improve our models. To assess if there is a structural basis for antagonistic potency, we compared the stability of H12 by its root mean square fluctuation (Fig. S11). In all the complexes, significant backbone fluctuations were observed in the region of C-terminus of H11, 11–12 loop, and H12, in comparison to complex with agonist testosterone, where RMSF only slightly deviated from the baseline. Thus, the closed conformation of H12, observed in the complex with an agonist, is significantly destabilized in complexes with compounds of interest. Structures of complexes with the most potent compounds **6** and **9** obtained by MD are shown on Fig. 3(C and D). As can be seen, ligands rotated in such a way that benzimidazole moiety comes into closer contact with helix 12. They also display putative hydrogen bonds between Asn705, Thr877, Gln711, ligand C17-substituent ring heteroatoms, and hydroxyl group at C3. Similar shift towards H12 was observed in complex with galeterone **2**, as well as hydrogen bond with Asn705, although overall positioning of heterocycle was different (Fig. S12-1). Compounds **5** and **8** displayed less tendency to shift towards H12, and reduced ability to form the mentioned hydrogen bonds (Fig. S12-2,3), therefore their conformation stayed closer to initial one shown on Fig. 3 (A,B), and they correspondingly produced slightly less disturbance in H12 region (Fig. S11).

Summarizing all the above, molecular dynamics simulation showed that compounds **5, 6, 8, 9** as well as galeterone, have an ability to destabilize the closed conformation of helix 12, which provides structural basis for antagonistic activity.

3.3. Inhibition of LNCap and PC-3 cells growth

We have found that all tested compounds slightly inhibited growth of prostate carcinoma LNCaP and PC-3 cells at 24 h incubation (in concentrations up to 100 μM), however some of the new compounds were significantly more active at 96 h incubation (Table 1). In discussion below, ANOVA.nls p-values are given in parentheses, and values below 0.05 indicate statistically significant differences between compound activities being compared.

Anti-proliferative activity of 16,17-unsaturated oxazoline **4** was considerably stronger than that of its saturated counterpart **7** ($p = 0.009$, LNCaP; $p = 0.002$, PC-3). 16,17-unsaturated benzimidazole **6** was also significantly more active than related saturated compound **9** ($p = 0.002$, LNCaP; $p = 0.004$, PC-3). Unsaturated benzoxazole **5** inhibited cells growth less potently than both 16,17-unsaturated, and 16,17-saturated oxazolines and benzimidazoles **4**, **6**, and **7** ($p \leq 0.037$, LnCaP; $p \leq 0.01$, PC-3). Benzoxazole **8** and oxazoline **10** did not exhibit significant anti-proliferative activity.

Activity of the two compounds, 2′-(3β-hydroxyandrosta-5,16-dien-17-yl)-4′,5′-dihydro-1′,3′-oxazole **4** and 2′-(3β-hydroxyandrosta-5,16-dien-17yl)-benzimidazole **6** significantly exceeded that of abiraterone and galeterone in LNCaP cells ($p \leq 0.025$). In PC-3 cells, compound **6**, despite having lower GI50, was probably on par with abiraterone and galeterone ($p \geq 0.05$), while compound **4** was significantly more potent ($p \leq 0.0009$).

4. Conclusions.

Synthesis of seven new steroidal oxazolines, benzoxazoles and benzimidazoles was performed. Docking of new compounds to CYP17 A1 revealed that structure of azole moiety and presence of Δ^{16} determine their positions in the active site of this enzyme. Molecular modeling of LBD AR complexes with benzoxazole and benzimidazole derivatives predicted that binding of aforementioned compounds should destabilize the “agonistic” conformation of H12, likewise in the case of galeterone binding. Five of the seven newly synthesized compounds possessed high anti-proliferative activity towards LNCaP and PC-3 prostate carcinoma cell lines, while two of them, 2’-(3β-hydroxyandrosta-5,16-dien-17-yl)-4’,5’-dihydro-1’,3’-oxazole **4** and 2’-(3β-hydroxyandrosta-5,16-dien-17yl)-benzimidazole **6**, were found to be the most potent inhibitors of LNCaP and PC-3 cells growth.

Acknowledgments

Authors are acknowledged to Maria G. Zavialova, fulfilling mass spectrometric measurements using the equipment of “Human

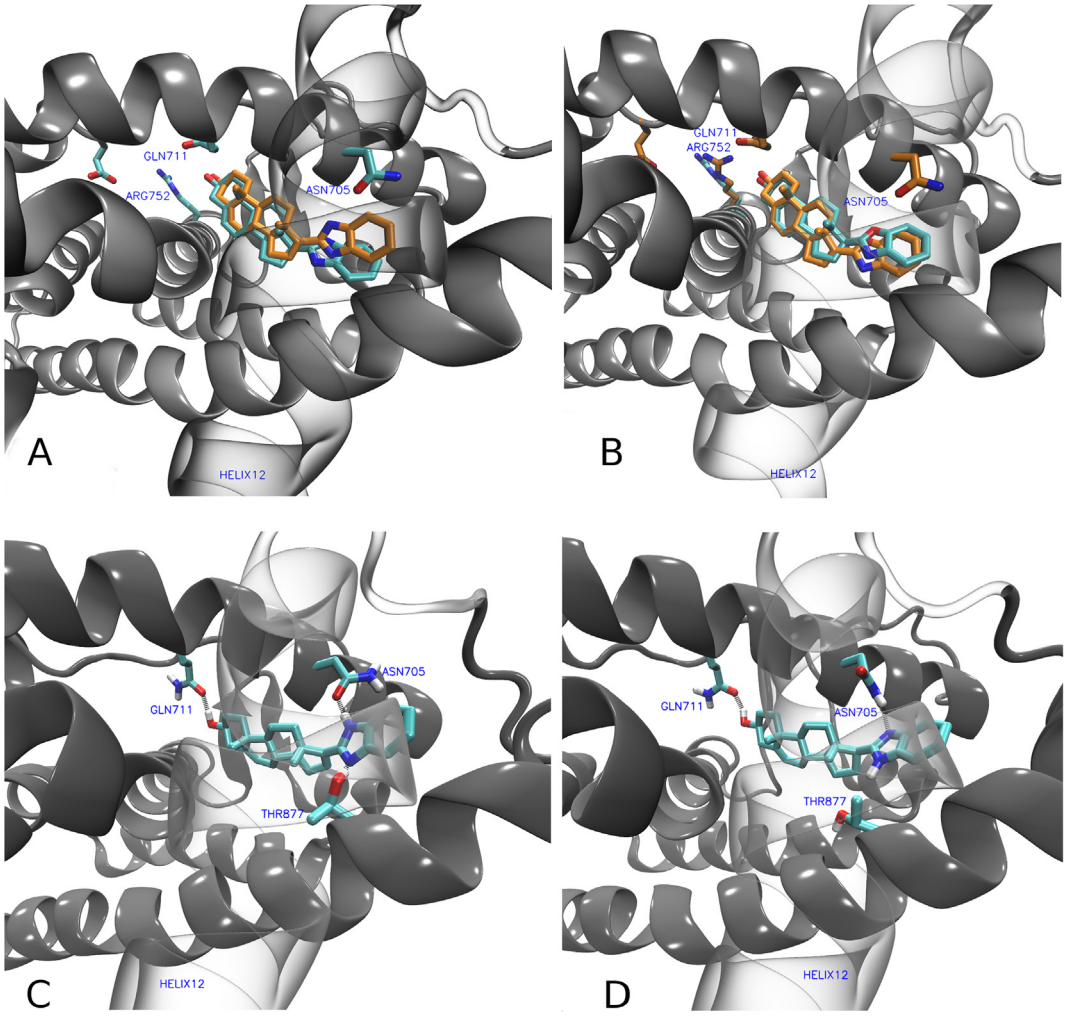

Fig. 3. Possible binding modes of compounds **5**, **6**, **8**, and **9**, to AR LBD. Receptor structures were generated by MD simulation, starting at 2AM9 crystal structure. Docking poses were pre-filtered by discarding ones with docking energy of 4 kcal/mol above best, and then lowest-energy conformations were selected from clusters with RMSD of the steroid skeleton close to one found in 2AM9. Resulting complexes were then subjected to 300 ns MD equilibration; then, structures corresponding to the most stable clusters identified using DBSCAN algorithm were selected. Hydrogen bonds identified using distance cutoff of 3 Å, and donor-H-acceptor angle cutoff 30° are shown by dashed lines. A – docking pose for compounds **6** (orange) and **9** (cyan); B – docking pose for compounds **5** (orange) and **8** (cyan); C – complex of compound **6** after MD equilibration; D – complex of compound **9** after MD equilibration.

Table 1
Effects of Compounds **1 – 10** on Growth and Viability of LNCap and PC-3 Cells (GI_{50} ± SE, μM) at 96 h Incubation.

Compound	LNCaP	PC-3
Abiraterone 1	22.6 ± 4.9	17.2 ± 5.2
Galeterone 2	10.6 ± 2.0	10.8 ± 1.8
3	24.9 ± 8.3	14.4 ± 4.9
4	3.7 ± 0.6	2.3 ± 0.6
5	28.8 ± 7.1	33.6 ± 9.6
6	3.8 ± 1.1	6.9 ± 1.3
7	11.6 ± 3.6	10.7 ± 2.6
8	n.d.*	n.d.*
9	20.8 ± 4.70	20.1 ± 3.6
10	n.d.*	n.d.*

*Subtle effect on proliferation at some concentrations; parameters determined by fitting Hill's equation to data were not statistically significant ($p > 0.05$).

Proteome" Core Facilities (Institute of Biomedical Chemistry, Moscow, Russia) and to Dmitry N. Kaluzhny (Engelhardt Institute of Molecular Biology) for recording of CD spectra. Authors also thank the Program of fundamental research for state academies for 2013–2020 years (No 01201363817) for support of NMR studies in Engelhardt Institute of Molecular Biology RAS (R.A.N., Y.V.T, V.P.T). The chemical synthesis and biological studies of new compounds were supported by Russian Scientific Foundation RSF grant 18-75-10008 (A.S.L, V.A.Z, V.S.P.); molecular modeling studies were supported by Russian Foundation for Basic Research and Government of Moscow grant 19-34-70023 (Y.V.T.).

Appendix A. Supplementary data

Supplementary data to this article can be found online at https://doi.org/10.1016/j.steroids.2019.108534.

References

[1] V.C. Njar, A.M. Brodie, Inhibitors of 17α-hydroxylase/17,20-lyase (CYP17) potential agents for the treatment of prostate cancer, Curr. Pharm. Des. 5 (1999) 163–180.
[2] R.W. Hartmann, P.B. Ehmer, S. Haidar, M. Hector, J. Jose, C.D. Klein, S.D. Seidel, T.F. Sergejew, B.G. Wachall, G.A. Wächter, Y.P. Zhuang, Inhibition of CYP 17, a new strategy for the treatment of prostate cancer, Arch. Pharm. Med. Chem. 4 (2002) 119–128.
[3] R.D. Bruno, V.C.O. Njar, Targeting cytochrome P450 enzymes: a new approach in anti-cancer drug development, Bioorg. Med. Chem. 15 (2007) 5047–5060.
[4] E. Baston, F.R. Leroux, Inhibitors of steroidal cytochrome P450 enzymes as targets for drug development, Rec. Pat. Anticancer Drug Disc. 2 (2007) 31–58.
[5] V.M. Moreira, J.A.R. Salvador, T.S. Vasaitis, V.C. Njar, CYP17 Inhibitors for prostate

cancer treatment – an update, Curr. Med. Chem. 15 (2008) 868–899.
[6] C.P. Owen, 17α-Hydroxylase/17,20-lyase ($P450_{17\alpha}$) inhibitors in the treatment of prostate cancer, Anti-Cancer Agents Med. Chem. 9 (2009) 613–626.
[7] T.S. Vasaitis, R.D. Bruno, V.C.O. Njar, CYP17 inhibitors for prostate cancer therapy, J. Steroid Biochem. Mol. Biol. 125 (2011) 23–31.
[8] J.A.R. Salvador, R.M.A. Pinto, S.M. Silvestre, Steroidal 5α-reductase and 17α-hydroxylase/17,20-lyase (CYP17) inhibitors useful in the treatment of prostatic diseases, J. Steroid Biochem. Mol. Biol. 137 (2013) 199–222.
[9] G.A. Potter, S.E. Barrie, M. Jarman, M.G. Rowlands, Novel steroidal inhibitors of human cytochrome P45017 alpha (17alpha-hydroxylase-C17,20-lyase): potential agents for the treatment of prostatic cancer, J. Med. Chem. 38 (1995) 2463–2471.
[10] R.D. Bruno, T.S. Vasaitis, L.K. Gediya, P. Purushottamachar, A.M. Godbole, Z. Ates-Alagoz, A.M. Brodie, V.C.O. Njar, Synthesis and biological evaluations of putative metabolically stable analogs of VN/124-1 (TOK-001): head to head anti-tumor efficacy evaluation of VN/124-1 (TOK- 001) and abiraterone in LAPC-4 human prostate cancer xenograft model, Steroids 76 (2011) 1268–1279.
[11] V.D. Handratta, T.S. Vasaitis, V.C.O. Njar, L.K. Gediya, R. Kataria, P. Chopra, D. Newman Jr, R. Farquhar, Z. Guo, Y. Qiu, A.M.H. Brodie, Novel C-17-heteroaryl steroidal CYP17 inhibitors/antiandrogens: synthesis, in vitro biological activity, pharmacokinetics, and antitumor activity in the LAPC4 human prostate cancer xenograft model, J. Med. Chem. 48 (2005) 2972–2984.
[12] V.C.O. Njar, A.M.H. Brodie, Discovery and development of Galeterone (TOK-001 or VN/124-1) for the treatment of all stages of prostate cancer, J. Med. Chem. 58 (2015) 2077–2087.
[13] N.M. DeVore, E.E. Scott, Cytochrome P450 17A1 structures with prostate cancer drugs Abiraterone and TOK-001, Nature 482 (7383) (2012) 116–119.
[14] F. Xiao, M. Yang, Y. Xu, W. Vongsangnak, Comparisons of prostate cancer inhibitors Abiraterone and TOK-001 binding with CYP17A1 through Molecular Dynamics, Comp. Struct. Biotechnol. J. 13 (2015) 520–527.
[15] E. Gianti, R.J. Zauhar, Modeling androgen receptor flexibility: a binding mode hypothesis of CYP17 inhibitors/antiandrogens for prostate cancer therapy, J. Chem. Inf. Model. 52 (2012) 2670–2683.
[16] H. Grossebrummel, T. Peter, R. Mandelkow, M. Weiss, D. Muzzio, U. Zimmermann, R. Walther, F. Jensen, C. Knabbe, M. Zygmunt, M. Burchardt, M.B. Stope, Cytochrome P450 17A1 inhibitor abiraterone attenuates cellular growth of prostate cancer cells independently from androgen receptor signaling by modulation of oncogenic and apoptotic pathways, Int. J. Oncol. 48 (2016) 793–800.
[17] R.D. Bruno, T.D. Gover, A.M. Burger, A.M.H. Brodie, V.C.O. Njar, 17α-Hydroxylase/17,20-lyase inhibitor VN/124-1 inhibits growth of androgen-independent prostate cancer cells via induction of the endoplasmic reticulum stress response, Mol. Cancer Ther. 7 (2008) 2828–2836.
[18] A.K. Kwegyir-Afful, R.D. Bruno, P. Purushottamachar, F.N. Murigi, V.C.O. Njar, Galeterone and VNPT55 disrupt Mnk-eIF4E to inhibit prostate cancer cell migration and invasion, FEBS J 283 (2016) 3898–3918.
[19] S. Ramalingam, V.P. Ramamurthy, V.C.O. Njar, Dissecting major signaling pathways in prostate cancer development and progression: Mechanisms and novel therapeutic targets, J Steroid Biochem Mol Biol 166 (2017) 16–27.
[20] J.J. Ajdukovic, E.A. Djurendic, E.T. Petri, O.R. Klisuric, A.S. Celic, M.N. Sakač, D.S. Jakimov, K.M. Penov Gaši, 17(E)-Picolinylidene androstane derivatives as potential inhibitors of prostate cancer cell growth: antiproliferative activity and molecular docking studies, Bioorg Med. Chem. 21 (2013) 7257–7266.
[21] N. Szabó, J.J. Ajduković, E.A. Djurendić, M.N. Sakač, I. Ignáth, J. Gardi, G. Mahmoud, O.R. Klisurić, S. Jovanović-Šanta, K.M. Penov, K.M. Gaši, M. Szécsi, Determination of 17α-hydroxylase-C17,20-lyase (P450 17α) enzyme activities and their inhibition by selected steroidal picolyl and picolinylidene compounds, Acta Biol. Hung. 66 (2015) 41–51.
[22] A.V. Kuzikov, N.O. Dugin, S.V. Stulov, D.S. Shcherbinin, M.S. Zharkova, Y.V. Tkachev, V.P. Timofeev, A.V. Veselovsky, V.V. Shumyantseva, A.Y. Misharin, Novel oxazolinyl derivatives of pregna-5,17(20)-diene as 17a-hydroxylase/17,20-lyase (CYP17A1) inhibitors, Steroids 88 (2014) 66–71.
[23] V.A. Kostin, V.A. Zolottsev, A.V. Kuzikov, R.A. Masamrekh, V.V. Shumyantseva, A.V. Veselovsky, S.V. Stulov, R.A. Novikov, V.P. Timofeev, A.Y. Misharin, Oxazolinyl derivatives of [17(20)*E*]-21-norpregnene differing in the structure of A and B rings. Facile synthesis and inhibition of Cyp17A1 catalytic activity, Steroids 115 (2016) 114–122.
[24] V.A. Zolottsev, Y.V. Tkachev, A.S. Latysheva, V.A. Kostin, R.A. Novikov, V.P. Timofeev, G.E. Morozevich, A.V. Kuzikov, V.V. Shumyantseva, A.Y. Misharin, Comparison of [17(20)*E*]-21-norpregnene oxazolinyl and benzoxazolyl derivatives as inhibitors of CYP17A1 activity and prostate carcinoma cells growth, Steroids 129 (2018) 24–34.
[25] N. Zhu, Y. Ling, X. Lei, V. Handratta, A.M.H. Brodie, Novel $P450_{17\alpha}$ inhibitors: 17-(2'-oxazolyl)- and 17-(2'-thiazolyl)-androstene derivatives, Steroids 68 (2003) 603–611.
[26] J. Staunton, E.J. Eisenbraun, 3β-Acetoxyetienic acid [3β-Acetoxy-5-androstene-17β-carboxylic acid], Org. Synth. Coll. 5 (1973) 8, https://doi.org/10.15227/orgsyn.042.0004.
[27] D.J. Price, C.L. Brooks, A modified TIP3P water potential for simulation with Ewald summation, J. Chem. Phys. 121 (2004) 10096–10103, https://doi.org/10.1063/1.1808117.
[28] S. Nosé, A unified formulation of the constant temperature molecular-dynamics methods, J. Chem. Phys. 81 (1984) 511–519, https://doi.org/10.1063/1.447334.
[29] M. Parrinello, A. Rahman, Polymorphic transitions in single crystals: a new molecular dynamics method, J. Appl. Phys. 52 (1981) 7182–7190, https://doi.org/10.1063/1.328693.
[30] A.D. MacKerell Jr, M. Feig, C.L. Brooks III, Extending the treatment of backbone energetics in protein force fields: limitations of gas-phase quantum mechanics in reproducing protein conformational distributions in molecular dynamics simulations, J. Comp. Chem. 25 (2004) 1400–1415, https://doi.org/10.1002/jcc.20065.
[31] D. van der Spoel, E. Lindahl, B. Hess, G. Groenhof, A.E. Mark, H.J.C. Berendsen, GROMACS: fast, flexible and free, J. Comp. Chem. 26 (2005) 1701–1719, https://doi.org/10.1002/jcc.20291.
[32] V. Zoete, M.A. Cuendet, A. Grosdidier, O. Michielin, SwissParam,, a fast force field generation tool for small organic molecules, J. Comput. Chem. 32 (2011) 2359–2368, https://doi.org/10.1002/jcc.21816.
[33] W. Humphrey, A. Dalke, K. Schulten, VMD: Visual molecular dynamics, J. Mol. Graph. 14 (1996) 33–38, https://doi.org/10.1016/0263-7855(96)00018-5.
[34] O. Trott, A.J. Olson, AutoDock Vina: improving the speed and accuracy of docking with a new scoring function, efficient optimization and multithreading, J. Comput. Chem. 31 (2010) 455–461, https://doi.org/10.1002/jcc.21334.
[35] R.J.G.B. Campello D. Moulavi J. Sander Density-based clustering based on hierarchical density estimates Lecture Not. Comput. Sci. 7819 2013 160 172 10.1007/978-3-642-37456-2_14.
[36] T. Mosmann, Rapid colorimetric assay for cellular growth and survival: application to proliferation and cytotoxicity assays, J. Immunol. Methods 65 (1983) 55–63.
[37] R. Reeve, J.R. Turner, Pharmacodynamic Models: Parameterizing the Hill Equation, Michaelis-Menten, the Logistic Curve, and Relationships Among These Models, J. Biopharmaceut. Stat. 23 (3) (2013) 648–661.
[38] C. Ritz, J.C. Streibig, Nonlinear Regression with R, Springer, New York, 2008.
[39] T. Ye, M.A. McKervey, Organic synthesis with α-diazo carbonyl compounds, Chem. Rev. 94 (1994) 1091–1160.
[40] S.I. Alaqeel, Synthetic approaches to benzimidazoles from o-phenylenediamine: a literature review, J. Saudi Chem. Soc. 21 (2017) 229–237.
[41] K. Niknam, A. Fatehi-Raviz, Synthesis of 2-substituted benzimidazoles and bis-benzimidazoles by microwave in the presence of alumina-methanesulfonic acid, J. Iran. Chem. Soc. 4 (2008) 438–443.
[42] O.O. Clement, C.M. Freeman, R.W. Hartmann, V.D. Handratta, T.S. Vasaitis, A.M.H. Brodie, V.C.O. Njar, Three dimensional pharmacophore modeling of human CYP17 inhibitors. Potential agents for prostate cancer therapy, J. Med. Chem. 46 (2003) 2345–2351.
[43] M.H. Tan, J. Li, H.E. Xu, K. Melcher, E.L. Yong, Androgen receptor: structure, role in prostate cancer and drug discovery, Acta Pharmacol. Sin. 36 (2015) 3–23, https://doi.org/10.1038/aps.2014.18.
[44] Sebastian Salentin, Sven Schreiber, V. Joachim Haupt, Melissa F. Adasme, Michael Schroeder, PLIP: fully automated protein–ligand interaction profiler, Nucleic Acids Res 43 (W1) (2015) W443–W447, https://doi.org/10.1093/nar/gkv315.